

Absence of breakdown of ferrodark solitons exhibiting snake instability

Xiaoquan Yu^{1,2,*} and P. B. Blakie²

¹Graduate School of China Academy of Engineering Physics, Beijing 100193, China

²Department of Physics, Centre for Quantum Science,

and Dodd-Walls Centre for Photonic and Quantum Technologies, University of Otago, Dunedin, New Zealand

We investigate the dynamical stability and real time dynamics of the two-types of ferrodark solitons (FDSs) which occur as topological magnetic domain walls in the easy-plane phase of a quasi-two-dimensional (2D) ferromagnetic spin-1 Bose-Einstein condensate. The type-I FDS has positive inertial mass and exhibits a single dynamical instability that generates in plane spin winding, causing polar-core spin vortex dipoles. The positive inertial mass leads to the elastic oscillations of the soliton under transverse perturbations. The type-II FDS has negative inertial mass and exhibits a snake instability and a spin-twist instability, with the latter involving the generation of out of plane spin winding. Distinct from the normal dynamics of negative mass solitons under long wave length transverse perturbations, the snake instability does not lead to the type-II FDS breaking down. Instead, segments of the type-II FDS convert to type-I and mass vortex dipoles are produced. The resulting hybridized-chain of the two soliton types and vortices exhibits complex 2D soliton dynamics at long times while the vortices remain confined and the topological structure of a magnetic domain wall is preserved.

Introduction— Dark solitons in a Bose-Einstein condensate (BEC) are unstable against transverse perturbations in high dimensions ($d > 1$) [1, 2], known as the snake instability. Such an instability is a general phenomenon and exists for topological solitons in various systems [3–9]. It has been demonstrated that the presence of the snake instability occurs when the inertial mass, which appears in the Newton equation describing one-dimensional (1D) soliton motion in superfluids [3, 10], is negative [11]. This is a consequence of the soliton energy decreasing with increasing the travel speed. Applying this equation to an element of a line soliton subject to long wavelength transverse perturbations: the acceleration direction is opposite to the restoring force, the amplitude of the transverse deformations amplify, and the soliton eventually breaks down into vortex dipoles [12]. Recently, two types of ferrodark solitons (FDSs), manifesting as kinks in the transverse magnetization $F_{\perp} \equiv F_x + iF_y$ (with the magnetic field along z), have been found in a ferromagnetic spin-1 BEC [13–15]. For type-I FDSs, the inertial mass is positive while for type-II FDSs it is negative [14]. Hence, it could be expected that a type-II FDS in a quasi-two-dimensional (2D) system fragments under long wavelength transverse perturbations.

In this Letter, however, we find that, instead of breaking down, type-II FDSs exhibit complex non-linear dynamics while preserving the magnetic domain wall structure. We study the dynamical instabilities and dynamics of FDSs in a quasi-2D spin-1 BEC. For type-II FDSs, two dynamical instabilities are found, being a snake instability and a spin-twist instability. The unstable modes associated with the spin-twist instability generate spin-vortex dipoles in the $F_x - F_z$ plane. These spin-vortices are anomalous in that they do not have phase winding in the component wavefunctions. The amplitude of a long wavelength transverse perturbation to the type-II FDS grows at early times driven by the snake instability. This growth saturates at later time as elements reaching the propagating speed limit of FDSs convert to type-I FDSs. This leads to a hybridization of the soliton with spatially alternating type-I and type-II segments along its length, and $m = 0$

mass vortex dipole pairs produced at nodes of the motion and confined by the soliton. As a result, the hybridized FDS exhibits chaotic motion at long times without losing the domain wall topological structure in the transverse magnetization. In contrast, for the type-I FDSs, only the spin-twist instability exists and the combination of out-of-phase snake-like unstable modes in $m = \pm 1$ components produces polar-core spin-vortex dipole pairs in the $F_x - F_y$ plane. Since the inertial mass is positive, a type-I FDS oscillates under transverse perturbations, resembling the motion of an elastic string.

Spin-1 BECs — A spin-1 BEC consists of atoms with three hyperfine states $|F = 1, m = +1, 0, -1\rangle$ and is described by the three component wavefunction $\psi = (\psi_{+1}, \psi_0, \psi_{-1})^T$. The Hamiltonian density of a weakly interacting spin-1 BEC reads

$$\mathcal{H} = \frac{\hbar^2 |\nabla\psi|^2}{2M} + \frac{g_n}{2} |\psi^\dagger \psi|^2 + \frac{g_s}{2} |\psi^\dagger \mathbf{S} \psi|^2 + q \psi^\dagger S_z^2 \psi, \quad (1)$$

where M is the atomic mass, $g_n > 0$ is the density interaction strength, g_s is the spin-dependent interaction strength, $\mathbf{S} = (S_x, S_y, S_z)$, and $S_{j=x,y,z}$ are the spin-1 matrices [16, 17]. The uniform magnetic field is along the z -axis, and q denotes the quadratic Zeeman energy. The mean-field dynamics of the field ψ is governed by the Gross-Pitaevskii equations (GPEs)

$$\begin{aligned} i\hbar \frac{\partial \psi_{\pm 1}}{\partial t} &= [H_0 + g_s (n_0 + n_{\pm 1} - n_{\mp 1}) + q] \psi_{\pm 1} + g_s \psi_0^2 \psi_{\mp}^* \quad (2a) \\ i\hbar \frac{\partial \psi_0}{\partial t} &= [H_0 + g_s (n_{+1} + n_{-1})] \psi_0 + 2g_s \psi_0^* \psi_{+1} \psi_{-1}, \quad (2b) \end{aligned}$$

where $H_0 = -\hbar^2 \nabla^2 / 2M + g_n n$, $n_m = |\psi_m|^2$ and $n = \sum n_m$. The last terms on the right of Eqs. (2) describe the internal coherent spin exchange dynamics: $|00\rangle \leftrightarrow |+1\rangle |-1\rangle$ [18–20]. The magnetization density $\mathbf{F} \equiv \psi^\dagger \mathbf{S} \psi$ is the order parameter quantifying ferromagnetic $|\mathbf{F}| > 0$ for $g_s < 0$ (^{87}Rb , ^7Li) and anti-ferromagnetic order $\mathbf{F} = 0$ for $g_s > 0$ (^{23}Na) [16–20].

FDSs— The easy-plane phase of a uniform ferromagnetic ($g_s < 0$) spin-1 BEC is characterized by a transverse magnetization $\mathbf{F} \rightarrow F_{\perp} = F_{\perp}^g(\tau) = \sqrt{8n_{\pm 1}^b n_0^b} e^{i\tau}$, where $n_{\pm 1}^b =$

$(1 - \tilde{q})n_b/4$ and $n_0^b = n_b(1 + \tilde{q})/2$ are the component densities, n_b is the total number density, and $\tilde{q} \equiv -q/(2g_s n_b)$. Under constraint $F_z = n_{+1} - n_{-1} = 0$, this phase is the ground state for $0 < \tilde{q} < 1$ [16, 17]. The SO(2) symmetry of the easy-plane state is parameterized by the rotational angle about the z -axis τ . The FDS is a \mathbb{Z}_2 topological defect in the magnetic order of the easy-plane phase and connects regions transversely magnetized in opposite directions ($\tau = 0$ and $\tau = \pi$) [13–15]. In 1D, it is an Ising type kink and the corresponding magnetization $F_\perp(x)$ satisfies $F_\perp(-\infty) = F_\perp^s(\pi)$ and $F_\perp(+\infty) = F_\perp^s(0) = -F_\perp(-\infty)$. For $g_s = -g_n/2$ and $0 < \tilde{q} < 1$, exact FDS solutions to Eqs. (2) are available [14]. There are two types of such traveling kinks and the transverse magnetizations and the total number densities for speed V read

$$F_\perp^{I,II}(x, t) = e^{i\alpha} \sqrt{n_b^2 - \frac{q^2}{g_n^2} \tanh^2\left(\frac{x - Vt}{\ell^{I,II}}\right)}, \quad (3)$$

$$n^{I,II}(x, t) = n_b - \frac{g_n n_b - MV^2 \mp Q}{2g_n} \operatorname{sech}^2\left(\frac{x - Vt}{\ell^{I,II}}\right), \quad (4)$$

where $\ell^{I,II} = \sqrt{2\hbar^2/M(g_n n_b - MV^2 \mp Q)}$, and $Q = \sqrt{M^2 V^4 + q^2 - 2g_n M n_b V^2}$, and α is a rotational angle to parameterize the SO(2) symmetry. The $-$ ($+$) sign in front of Q specifies type-I (II) FDS. The upper bound of the traveling speed c_{FDS} is determined by $Q(V = c_{\text{FDS}}) = 0$ and this speed bound is markedly different from the group velocities of low-lying elementary excitations which normally set the speed limits of traveling defects [21]. Moreover, at $V = c_{\text{FDS}}$, the two types of FDSs do not vanish, but become identical [14].

The inertial mass is $M_{\text{in}} \equiv 2\partial\delta K/\partial V^2|_{V=0}$, where δK is the excitation energy of the soliton [3, 11]. Type-II FDSs have higher excitation energy (i.e. $\delta K^{\text{II}} > \delta K^{\text{I}}$), and δK^{I} increases monotonically with increasing V^2 , whereas δK^{II} decreases monotonically. Thus $M_{\text{in}}^{\text{I}} > 0$ and $M_{\text{in}}^{\text{II}} < 0$ [14]. Excitation energies of two types FDSs coincide smoothly at the maximum speed where transitions between the two types of FDSs could occur and induces oscillations of a FDS in hard-wall confined quasi-1D spin-1 BEC subject to a linear potential [14]. As we will see later, this property plays an essential role in 2D dynamics of FDSs.

Dynamical instabilities— Let us consider a straight infinitely long FDS along the y -axis located in the middle of a slab of width $L_s \gg \ell^{I,II}$. We consider a perturbed FDS $\psi = \psi_s + \delta\psi$, where ψ_s denote a stationary FDS ($V = 0$) and $\delta\psi = \epsilon[u(\mathbf{r})e^{-i\omega t} + v^*(\mathbf{r})e^{i\omega^* t}]$ is the perturbation with the dimensionless control parameter $\epsilon \ll 1$. Keeping leading order terms in Eq. (2) we obtain the Bogoliubov-de Gennes equations (BdGs):

$$\hbar\omega \begin{pmatrix} u \\ v \end{pmatrix} = \begin{pmatrix} \mathcal{L}_{\text{GP}} + X - \mu & \Delta \\ -\Delta^* & -(\mathcal{L}_{\text{GP}} + X - \mu)^* \end{pmatrix} \begin{pmatrix} u \\ v \end{pmatrix}, \quad (5)$$

where the stationary wavefunction satisfies $\mathcal{L}_{\text{GP}}\psi_s = \mu\psi_s$, $X = g_s \sum_{j=x,y,z} S_j \psi_s \psi_s^\dagger S_j + g_n \psi_s \psi_s^\dagger$, $\Delta = g_n \psi_s \psi_s^T + g_s \sum_{j=x,y,z} (S_j \psi_s)(S_j \psi_s)^T$ and $\mu = (g_n + g_s)n_b + q/2$ is the chemical potential. Since the system has translational symmetry

along the y -axis, we can use the wavevector k_y to parameterize the perturbations as $u(\mathbf{r}) = u(x)e^{ik_y y}$ and $v(\mathbf{r}) = v(x)e^{ik_y y}$. An imaginary part of energy $\hbar\omega$ marks a dynamical instability in the system, i.e., a mode that grows exponentially with time. Hereafter we choose $\alpha = 0$ for convenience and in which case $F_\perp = F_x$.

At $V = 0$ the wavefunctions of the exact FDSs are $\psi_s^{\text{I}} = \left(\sqrt{n_{\pm 1}^s} \tanh(x/2\ell^{\text{I}}), \sqrt{n_0^s}, \sqrt{n_{\pm 1}^s} \tanh(x/2\ell^{\text{I}})\right)^T$, $\psi_s^{\text{II}} = \left(\sqrt{n_{\pm 1}^s}, \sqrt{n_0^s} \tanh(x/2\ell^{\text{II}}), \sqrt{n_{\pm 1}^s}\right)^T$, and away from exactly solvable region, $\psi_s^{I,II}$ can be obtained numerically [15]. We numerically solve Eq. (5) with Neumann boundary conditions at x -axis boundaries [22]. For type-I FDSs, there is only one dynamical instability and the k_y region associated with the imaginary energy decreases as \tilde{q} increases [Fig. 1(a)]. The unstable mode leaves F_x unchanged and generates polar-core spin vortex dipole pairs in the (F_x, F_y) plane combined with modulations of F_z [Fig. 1(b)] and n [Fig. 1(c)]. We refer to this instability as type-I spin-twist instability. Interestingly, we see that this arises from the *out-of-phase combination* of snake-like unstable modes in $m = \pm 1$ components [Fig. 1(d),(e)].

For type-II FDSs, there exist two distinct unstable modes [Fig. 2(a)]. One unstable mode, which we refer to as the type-II spin-twist instability, creates spin vortex dipole pairs in the (F_x, F_z) plane accompanied by the modulations of F_y , while F_x is unchanged. Noticeably, in contrast to conventional spin vortices (polar core and Mermin-Ho vortices) [17], these spin-vortices are not generated by phase winding in components [Fig. 2(b)]. For given g_s/g_n , the unstable k_y region decreases monotonically as \tilde{q} increases and the imaginary energy vanishes at a certain value of \tilde{q} [Fig. 2(a)] [23]. The second unstable mode is a snake instability arising from the negative inertial mass of the type-II FDS. The imaginary energy as a function of k_y for this instability [see Fig. 2(a)] is similar to that for a dark soliton in scalar BECs [2]. For given g_s/g_n , the snake instability grows as q increases, since the distinction between two types of FDSs is greater for larger q [Fig. 2(a)]. The unstable mode resides dominantly in $m = 0$ state and creates transverse deformation of component density n_0 and vortex-dipole pairs [Fig. 2(d)(c)], a typical feature of the snake instability.

When $q \rightarrow 0$, $|M_{\text{in}}^{I,II}| \rightarrow +\infty$ [14], and the snake instability vanishes. In this limit, the system exhibits SO(3) rotational symmetry and the two types of FDSs are connected by a *symmetric* unitary spin-1 rotation ($\psi_s^{\text{II}} = U\psi_s^{\text{I}}$ and $U = U^T$) [13, 14] and consequently the two spin-twist unstable modes are also related by a spin rotation, namely, $u \rightarrow Uu$ and $v \rightarrow U^\dagger v$.

Absence of breakdown of type-II FDSs and proliferation of confined vortex dipoles— Let us now consider an open FDS in a spin-1 BEC confined by a hard-wall potential in a 2D square domain and study its real time dynamics. We initially impose a cosinusoidal transverse perturbation, with a system-size wavelength (much larger than the soliton width), to the FDS [Fig. 3 a(1)]. For a type-I FDS, since the inertial mass is

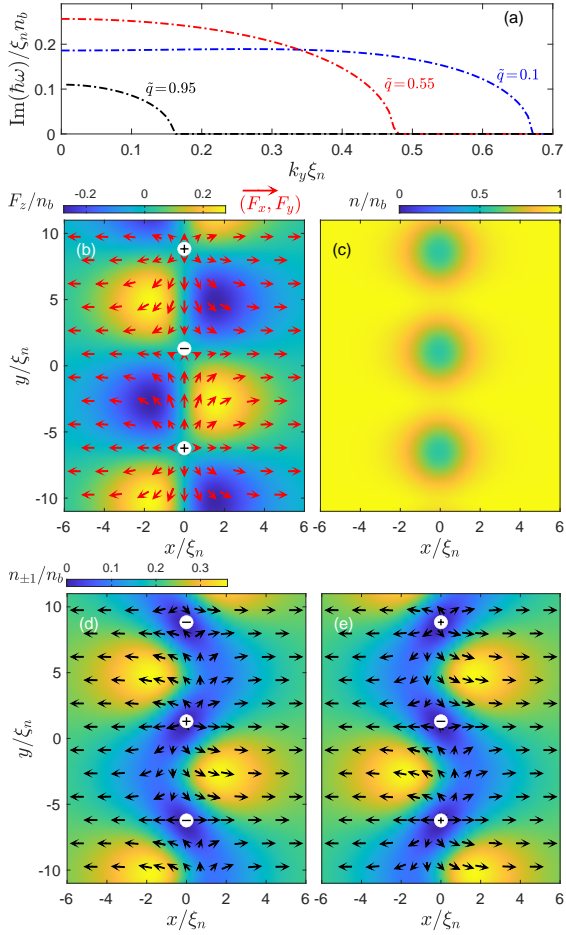


FIG. 1. Unstable modes associated with the spin-twist instability of type-I FDSs. (a) Imaginary of part of the spectrum of the unstable modes for $g_s/g_n = -0.5$ and $\tilde{q} = 0.1, 0.55, 0.95$. For the unstable mode [$\text{Im}(\hbar\omega) \neq 0$], the corresponding real part of the spectrum is zero. (b) Spin-texture created by the unstable mode. White circles with + and - indicate positive and negative circulation polar-core spin-vortices, respectively. The red arrows and the background color represent transverse magnetization field (F_x, F_y) and longitudinal magnetization F_z , respectively. Moving along y (at constant x) F_y modulates while F_x is constant. Here n_b is the ground state density and $\xi_n = \hbar/\sqrt{Mg_n n_b}$ is the density healing length. (c) Total density modulation created by the unstable modes. In (d) and (e), the background color represent the profile of n_{+1} and n_{-1} and the black arrows represent the phase of ψ_{+1} and ψ_{-1} , respectively. White circles indicate vortices in the components. The unstable modes in (b)-(e) are chosen at $k_y \xi_n \approx 0.417$, $\tilde{q} = 0.1$ and we use $\epsilon = 2$.

positive, it exhibits elastic oscillations [Fig. 3(a1)-(a5)] [25]. Applying the same transverse deformation to the type-II FDS (Fig. 3 [b(1)]), its dynamics are rather different: the magnitude of the transverse perturbation increases initially with time [Fig. 3 (b1)-(b3)], as an unavoidable consequence of the negative inertial mass and the snake instability [Fig. 2 (d)(e)]. We would normally expect that the type-II FDS breaks down at later times. However the initial linear growth of the amplitude saturates and subsequently the FDS enters a nonlinear regime. Significantly, the FDS topological structure persists without

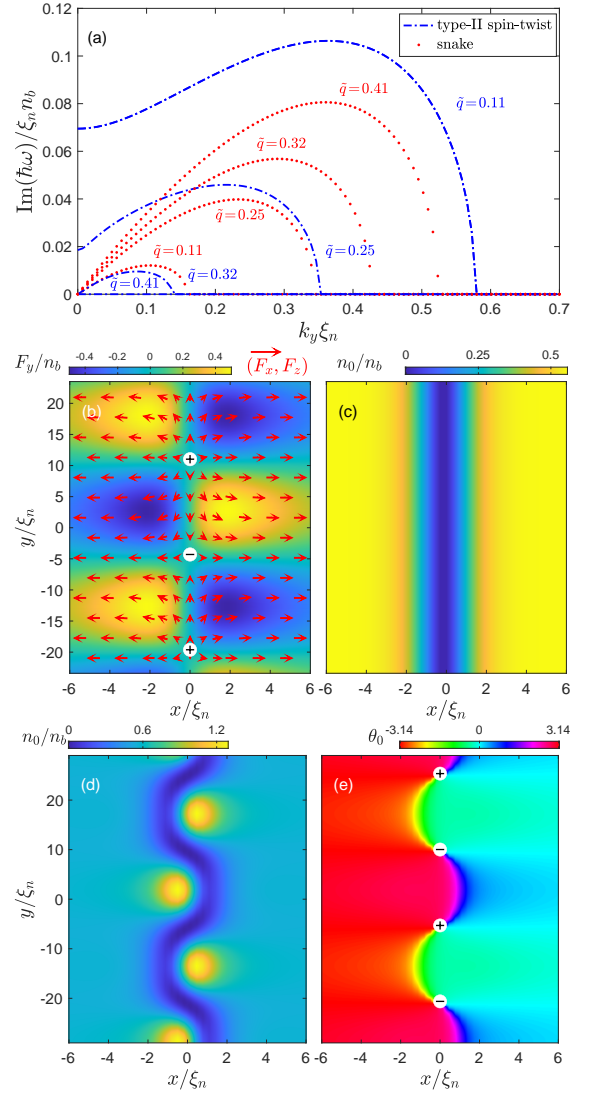


FIG. 2. Two unstable modes associated with type-II FDS (a) Imaginary of part of the spectrum of the unstable modes for $g_s/g_n = -1/2$ and $\tilde{q} = 0.11, 0.25, 0.32, 0.41$ (corresponding real part of the spectrum is zero). (b), (c) Effect of spin-twist unstable mode on the FDS. (b) White circles with + and - indicate positive and negative circulation of (F_x, F_z) spin-vortices, respectively. The red arrows and the background color represent magnetization fields (F_x, F_z) and F_y , respectively. (c) Component density n_0 is unaffected. (d), (e) Effect of snake unstable mode on the FDS. (d) Component density n_{+1} . (e) Phase θ_0 of the $m = 0$ component, with white circles indicating the circulation of ψ_0 component vortices. Accordingly, F_x is only spatially deformed and n_{+1} is weakly modulated (see Fig. S1(f)(g) [24]). The unstable modes in (b)-(e) are chosen at $k_y \xi_n \approx 0.205$, $\tilde{q} = 0.25$ and we use $\epsilon = 2$.

fragmenting into pieces and exhibits chaotic dynamics at late times [Fig. 3 (b6)-(b15)].

In order to examine the process of entering the nonlinear regime for an unstable type-II FDS, we consider a system that is periodic in the y direction (Fig. 4) for simplicity (to avoid the influence of boundaries). Let $x = x(y, t)$ be the position of the soliton core. The restoring force $F_r(y, t) = T\partial^2 x/\partial y^2$

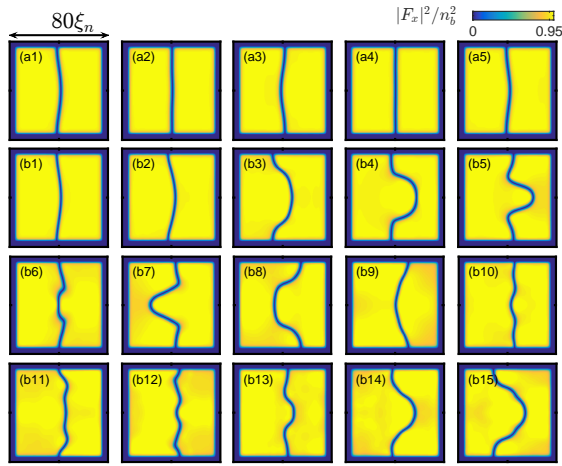


FIG. 3. Comparison between dynamics of open type-I and type-II FDSs with free end-points attached to the hard-wall boundaries, starting from initial states under the same transverse deformation [(a1) and (b1)]. The parameters are $g_s/g_n = -1/2$ and $\tilde{q} = 0.25$. The system is confined by hard-wall potentials in a square domain $x, y \in [-L, L]$ with $L = 40\xi_n$. The deformed profile is described by a cosine function. The time interval between snapshots is $60t_0$, where $t_0 = \hbar/g_n n_b$. (a1-a5) One period of evolution of the transversely deformed type-I FDS. (b1-b5) Evolution of a type-II FDS at the same times as in (a). (b6-b15) Subsequent time evolution after (b5).

and the acceleration $a_x(y, t) = \partial^2 x / \partial t^2$ have same sign for type-I FDSs and have opposite signs for type-II FDSs, where $T > 0$ is the “string” tension. At early times, the soliton is still a type-II FDS, and $F_r(y, t)$ and $a_x(y, t)$ have opposite signs [Fig. 4(e2)]. When a section of the soliton reaches the maximum speed, and it transfers into a type-I FDS locally, signaled by the corresponding part of $F_r(y, t)$ and $a_x(y, t)$ having same sign [Fig. 4(e3)]. At this stage the soliton forms a hybridized chain, with alternating line segments of type-I and type-II FDS character. At a later time the soliton transfers entirely to type-I FDS [Fig. 4(e4)] [26]. Additionally $m = 0$ mass vortex dipoles develop at the places where the soliton speed is zero [Fig. 4(c1)-(c5)]. Intriguingly, these $m = 0$ vortex dipoles are confined by the type-I FDS and do not become free. The complex nonlinear motion shown in Fig. 3 [(b6)-(b15)] can hence be understood as a result of a combination of a hybridized FDS and mass current generated by confined $m = 0$ vortex dipoles.

We emphasize that since the unstable modes of spin-twist instabilities keep F_x unchanged, the magnetic domain wall structure of both type-I and type-II FDSs do not break down under the corresponding perturbations. This is confirmed by numerical simulations of real time dynamics of FDS with initially imprinting the unstable modes associated with the spin twist instabilities (see Figs. S2 and S3 [24]).

Conclusion— We investigate dynamical instability and dynamics of 2D ferrodark solitons in a ferromagnetic spin-1 Bose-Einstein condensate. A type-II ferrodark soliton processes both snake and spin-twist instabilities. In contrast to the normal situation, however, in dynamics a type-II ferrodark

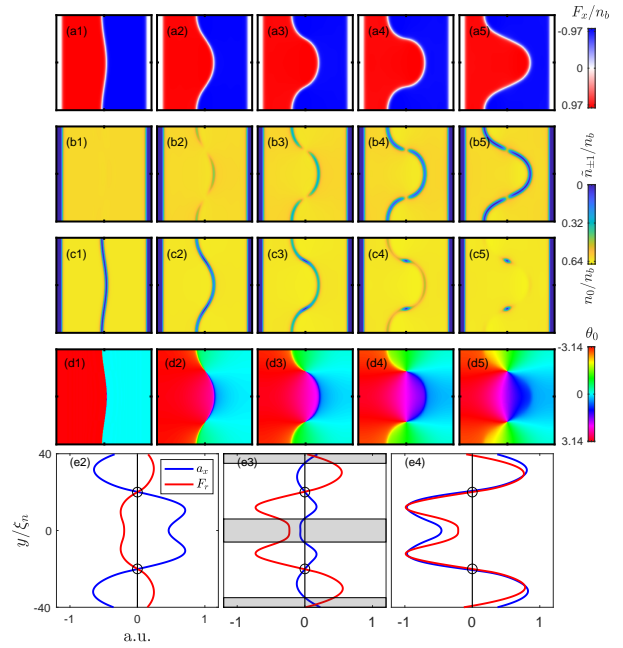


FIG. 4. Early time dynamics of a type-II FDS. The system is periodic in y and is confined by hard-wall potentials in x . The time interval between snapshots is $30t_0$. The initial transverse deformation and other parameters are as in Fig. 3. (a1)-(a5) Profile of the transverse magnetization F_x . The sign change of F_x across the core is kept during the motion. (b1)-(b5) and (c1)-(c5) dynamics of component densities $n_{\pm 1}$ and n_0 , respectively. Here $\tilde{n}_{\pm 1} = n_{\pm 1} \bar{n}_0 / \bar{n}_{\pm 1}$ is re-scaled component density and \bar{n}_0 and $\bar{n}_{\pm 1}$ are ground state component densities. (d1)-(d5) The phase of $m = 0$ spin state, showing proliferation of a mass vortex dipole in $m = 0$ component [(d4),(d5)]. (e2)-(e4) Acceleration (blue line) and restoring force (red line) at evolution stages (2), (3) and (4). In (e3), F_r and a_x have the same sign in the shaded region. The values of F_r and a_x are in arbitrary units and are scaled within $[-1, 1]$ for convenience. The black circles mark positions of nodes $[(0, -L/4), (0, L/4)]$ which coincide with the positions of $m = 0$ vortices.

soliton does not fragment under transverse perturbations and instead exhibits complex motion accompanied by forming a hybridized chain of type-I and type-II ferrodark soliton with a proliferation of confined $m = 0$ vortex dipole pairs. A type-I ferrodark soliton exhibits oscillations under transverse perturbations [27] and the relevant unstable mode creates polar-core spin-vortex dipoles. This work explores rich phenomena of 2D soliton instability and dynamics [28] which have not been encountered in the past and will motivate further theoretical studies. Moreover, experimental investigations are also within the scope of current ultracold-gas experiments [8, 9, 29–34].

Acknowledgment— We thank M. Antonio, D. Baillie and for useful discussions. X.Y. acknowledges support from the National Natural Science Foundation of China (Grant No. 12175215), the National Key Research and Development Program of China (Grant No. 2022YFA 1405300) and NSF (Grant No. U2330401). P.B.B acknowledges support from the Marsden Fund of the Royal Society of New Zealand.

* xqyu@gscaep.ac.cn

- [1] E. Kuznetsov and S. Turitsyn, *Zh. Eksp. Teor. Fiz* **94**, 129 (1988).
- [2] A. E. Muryshev, H. B. van Linden van den Heuvell, and G. V. Shlyapnikov, *Phys. Rev. A* **60**, R2665 (1999).
- [3] R. G. Scott, F. Dalfovo, L. P. Pitaevskii, and S. Stringari, *Phys. Rev. Lett.* **106**, 185301 (2011).
- [4] A. Gallemí, L. P. Pitaevskii, S. Stringari, and A. Recati, *Phys. Rev. A* **100**, 023607 (2019).
- [5] C. Qu, M. Tylutki, S. Stringari, and L. P. Pitaevskii, *Phys. Rev. A* **95**, 033614 (2017).
- [6] S. S. Shamaïlov and J. Brand, *SciPost Phys.* **4**, 18 (2018).
- [7] C. Qu, L. P. Pitaevskii, and S. Stringari, *Phys. Rev. Lett.* **116**, 160402 (2016).
- [8] A. Farolfi, D. Trypogeorgos, C. Mordini, G. Lamporesi, and G. Ferrari, *Phys. Rev. Lett.* **125**, 030401 (2020).
- [9] X. Chai, D. Lao, K. Fujimoto, R. Hamazaki, M. Ueda, and C. Raman, *Phys. Rev. Lett.* **125**, 030402 (2020).
- [10] V. V. Konotop and L. Pitaevskii, *Phys. Rev. Lett.* **93**, 240403 (2004).
- [11] A. M. Kamchatnov and L. P. Pitaevskii, *Phys. Rev. Lett.* **100**, 160402 (2008).
- [12] G. Huang, V. A. Makarov, and M. G. Velarde, *Phys. Rev. A* **67**, 023604 (2003).
- [13] X. Yu and P. B. Blakie, *Phys. Rev. Research* **3**, 023043 (2021).
- [14] X. Yu and P. B. Blakie, *Phys. Rev. Lett.* **128**, 125301 (2022).
- [15] X. Yu and P. B. Blakie, *Phys. Rev. Res.* **4**, 033056 (2022).
- [16] D. M. Stamper-Kurn and M. Ueda, *Rev. Mod. Phys.* **85**, 1191 (2013).
- [17] Y. Kawaguchi and M. Ueda, *Phys. Rep.* **520**, 253 (2012), spinor Bose–Einstein condensates.
- [18] T.-L. Ho, *Phys. Rev. Lett.* **81**, 742 (1998).
- [19] T. Ohmi and K. Machida, *J. Phys. Soc. Jpn* **67**, 1822 (1998).
- [20] L. E. Sadler, J. M. Higbie, S. R. Leslie, M. Vengalattore, and D. M. Stamper-Kurn, *Nature* **443**, 312 (2006).
- [21] L. Pitaevskii and S. Stringari, *Bose-Einstein condensation and superfluidity*, Vol. 164 (Oxford University Press, 2016).
- [22] Note that the unstable modes must be localized in space and are insensitive to boundary conditions as long as $L_s \gg \ell^{II}$.
- [23] For small spin coupling strength $|g_s/g_n| \lesssim 0.1$, the spin-twist instability persists in the whole easy-plane phase ($0 < \tilde{q} < 1$).
- [24] See Supplemental Material for details.
- [25] Positive inertial mass does not necessarily ensure stable oscillations. This is the case for long phase domain walls [35], whose inertial mass is positive for weak coherent coupling strengths [4–6], which have been shown to fragment under evolution [4, 36].
- [26] It is worthwhile mentioning that once a hybridized FDS is formed, transition between two types may happen through a longitudinal motion of the interface between the two types along the soliton line and the condition of reaching the maximum speed is not necessarily fulfilled for the transition to occur. As seen in Fig. 4(e4), at that time the whole FDS converts to type-I and the elements near the locations of the vortices have never moved at the speed limit.
- [27] The dependence on the inertial mass of the oscillation frequency remains an interesting question to resolve, especially in the $q \rightarrow 0$ limit where the conservation law of magnetization may play an important role [13].
- [28] The relevant characteristic features of FDSs revealed by the presented results on the strong spin interaction regime hold for $0 < |g_s/g_n| < 1$.
- [29] L. Chomaz, L. Corman, T. Bienaimé, R. Desbuquois, C. Weitenberg, S. Nascimbène, J. Beugnon, and J. Dalibard, *Nat. Commun.* **6** (2015).
- [30] G. Gauthier, I. Lenton, N. M. Parry, M. Baker, M. J. Davis, H. Rubinsztein-Dunlop, and T. W. Neely, *Optica* **3**, 1136 (2016).
- [31] G. Semeghini, G. Ferioli, L. Masi, C. Mazzinghi, L. Wolswijk, F. Minardi, M. Modugno, G. Modugno, M. Inguscio, and M. Fattori, *Phys. Rev. Lett.* **120**, 235301 (2018).
- [32] J. M. Higbie, L. E. Sadler, S. Inouye, A. P. Chikkatur, S. R. Leslie, K. L. Moore, V. Savalli, and D. M. Stamper-Kurn, *Phys. Rev. Lett.* **95**, 050401 (2005).
- [33] S. Huh, K. Kim, K. Kwon, and J.-y. Choi, *Phys. Rev. Research* **2**, 033471 (2020).
- [34] M. Prüfer, D. Spitz, S. Lannig, H. Strobel, J. Berges, and M. K. Oberthaler, *Nature Physics* **18**, 1459 (2022).
- [35] D. T. Son and M. A. Stephanov, *Phys. Rev. A* **65**, 063621 (2002).
- [36] K. Ihara and K. Kasamatsu, *Phys. Rev. A* **100**, 013630 (2019).

Supplemental Material for “ Absence of breakdown of ferrodark soltions exhibiting snake instability ”

UNSTABLE MODES ASSOCIATED WITH THE SNAKE INSTABILITY

Unstable modes associated with the snake instability for type-II FDSs generate spatial deformation of F_x and weak modulation of $n_{\pm 1}$. The magnetization F_x is always zero at the core and the sign change of F_x remains unchanged across the core.

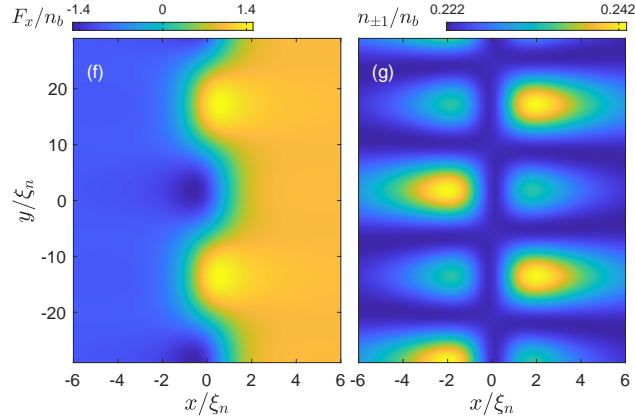


FIG. S1. Profiles of F_x and $n_{\pm 1}$ created by the unstable modes associated with the snake instability. The unstable modes are chosen at $k_y \xi_n \simeq 0.205$, $\tilde{q} = 0.25$ and we use $\epsilon = 2$.

DYNAMICS OF FERRODARK SOLITONS PERTURBED BY THE SPIN-TWIST UNSTABLE MODES

The initial state is the perturbed wavefunction $\psi = \psi_s + \delta\psi$, where ψ_s is the wavefunction of a stationary FDS and $\delta\psi = \epsilon[u(\mathbf{r})e^{-i\omega t} + v^*(\mathbf{r})e^{i\omega^* t}]$ is the perturbation contributed by the unstable mode associated with the spin-twist instability. Figures S2 and S3 show the real time dynamics of a type-I FDS and a type-II FDS, respectively.

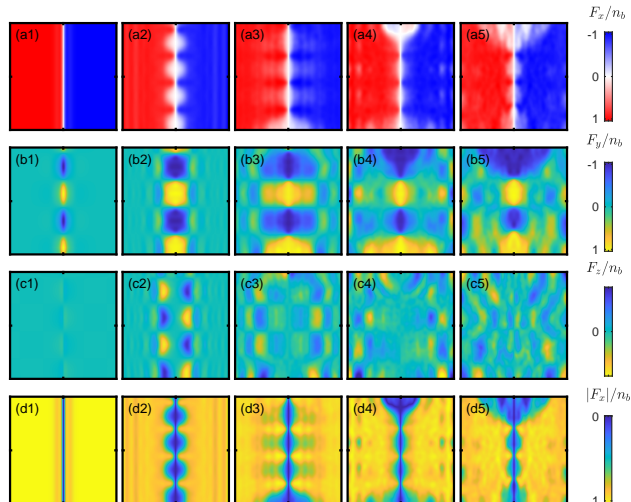


FIG. S2. Time evolution of a type-I FDS which is initially perturbed by the unstable mode associated with the type-I spin-twist instability. (a1)-(a5), (b1)-(b5), and (c1)-(c5) show the time evolution of F_x , F_y and F_z , respectively. (d1)-(d5) The corresponding profile of $|F_x|$. The system is in a square domain $x, y \in [-L, L]$ with $L = 40\xi_n$. Here $g_s/g_n = -1/2$, $\tilde{q} = 0.1$, and Neumann boundary condition is applied. The time interval between snapshots is $40t_0$. The unstable modes are chosen at $k_y \xi_n \simeq 0.1556$ and we use $\epsilon = 0.1$.

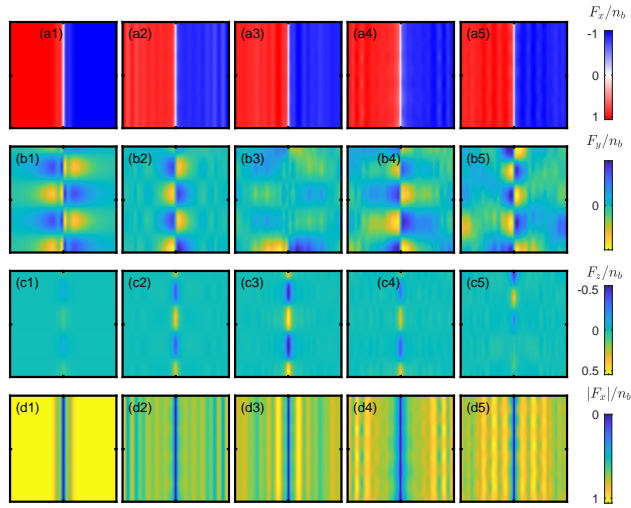


FIG. S3. Time evolution of a type-II FDS which is initially perturbed by the unstable mode associated with the type-II spin-twist instability. (a1)-(a5), (b1)-(b5), and (c1)-(c5) show the time evolution of F_x , F_y and F_z , respectively. (d1)-(d5) The corresponding profile of $|F_x|$. The unstable modes are chosen at $k_y \xi_n \simeq 0.1556$, $\tilde{q} = 0.25$ and we use $\epsilon = 0.2$. The system size, the interaction strength, the time interval between each snapshot, and the boundary condition are the same as in Fig. S2.